Available online at www.sciencedirect.com
SCIENCE DIRECT®
Journal of Chromatography A, 1063 (2005) 47–56
JOURNAL OF CHROMATOGRAPHY A
www.elsevier.com/locate/chroma

# Evaluation of nonlinear chromatographic performance by frontal analysis using a simple multi-plate mathematical model

Weiqiang Hao, Junde Wang*

*Dalian Institute of Chemical Physics, Chinese Academy of Sciences, 161 Zhongshan Road, Dalian 116012, PR China*

Received 5 March 2004; received in revised form 19 November 2004; accepted 19 November 2004
Available online 10 December 2004

**Abstract**

A multi-plate (MP) mathematical model was proposed by frontal analysis to evaluate nonlinear chromatographic performance. One of its advantages is that the parameters may be easily calculated from experimental data. Moreover, there is a good correlation between it and the equilibrium-dispersive (E-D) or Thomas models. This shows that it can well accommodate both types of band broadening that is comprised of either diffusion-dominated processes or kinetic sorption processes. The MP model can well describe experimental breakthrough curves that were obtained from membrane affinity chromatography and column reversed-phase liquid chromatography. Furthermore, the coefficients of mass transfer may be calculated according to the relationship between the MP model and the E-D or Thomas models.


*Keywords:* Frontal analysis; Multi-plate model; Equilibrium-dispersive model; Thomas model; Membrane affinity chromatography; Reversed-phase liquid chromatography; Bovine serum albumin; Caffeine

## 1. Introduction

Frontal analysis (FA) is a useful method for chromatographic studies. Compared to another one, the pulse method, FA method is more suited for preparative chromatography where maximum usage of the adsorbent is desirable. Particularly for many preparative affinity separations, the assumption of a linear adsorption isotherm, which derived analytical solutions describing the chromatographic performance, is not applicable. In these cases, FA is usually considered as the preferred method [1–3].

FA has been widely applied to determine adsorption isotherms from breakthrough curves that are obtained at different feed concentrations of the adsorbate [4–9]. As its inverse problem, the breakthrough curve may be predicted when the isotherm is already known. Because the shape of the breakthrough curve can also be influenced by factors such as dispersion and sorption kinetics, this study will provide information about the process and then be helpful to optimize the operation [3,10,11]. For this purpose, Chase [1] had described a theoretical approach of FA to predict the performance of preparative affinity separations in packed columns. Suen and co-workers [12–14] proposed a mathematical model for FA to analyze the design and operation of affinity membrane bioseparations. Recently, Miyabe and Guiochon [15] proposed a FA method to measure the lumped mass transfer rate coefficient ($k_{m,L}$) in column reversed-phase liquid chromatography.

The equilibrium-dispersive (E-D) [7,15] and Thomas models [1,12,16] have been widely applied to FA. The E-D model lumps all contributions leading to band broadening into an apparent dispersion coefficient, $D$, and the Thomas model lumps those into an association rate coefficient, $k_1$. These coefficients may be used to indicate the chromatographic performance. In practice, $D$ and $k_1$ may be estimated by comparing experimental curves and theoretical ones that are calculated by changing the values of the coefficients [15]. In some cases, however, this procedure turns out to be arbitrary because there was usually a little discrepancy between experimental and theoretical values [14,15,17,18]. In these cases, some effects for band broadening turn not to be lumped

* Corresponding author. Tel.: +86 411 83693506; fax: +86 411 83693512.
*E-mail address:* wjd@dicp.ac.cn (J. Wang).

0021-9673/$ – see front matter © 2004 Elsevier B.V. All rights reserved.
doi:10.1016/j.chroma.2004.11.065

into $D$ and $k_1$. In addition, solving these models needs numerical methods and it will involve a great number of repeated computations. This makes the work of the calculation be somewhat large, and it seems not to be handy for chromatographers especially without computing ground.

In this paper, we propose a new mathematical model, the multi-plate (MP) model, for the FA method. It is expected to be capable of describing the breakthrough curve and also handy for chromatographers. As validation for its practical use, two different chromatographic systems, column reversed-phase liquid chromatography (RPLC) and membrane affinity chromatography (MAC) were performed. In the former, the E-D model has been widely applied due to the fact that fast equilibrium of the adsorbate between the mobile and stationary phases usually occurs. In the latter, the Thomas model turns out to be more appropriate because the slow sorption kinetics is the limiting factor. By applying the MP model to describe the breakthrough curves obtained in RPLC and MAC, it is shown that this model may be used to obtain information about band broadening effects.

## 2. Theoretical

### 2.1. Multi-plate model

In general, the chromatographic process may also be considered as occurring in series of theoretical plates [19]. For the FA method, in each plate, according to that the amount of the solute entering the plate is the sum of that leaving and the increment in mobile and stationary phases, the mass balance equation may be expressed as:

$$C_0\,\mathrm{d}V - C_1\,\mathrm{d}V = \frac{V_\mathrm{m}(1-\varepsilon)}{N}\,\mathrm{d}C_{\mathrm{s},1} + \frac{V_\mathrm{m}\varepsilon}{N}\,\mathrm{d}C_1 \tag{1a}$$

$$C_{i-1}\,\mathrm{d}V - C_i\,\mathrm{d}V = \frac{V_\mathrm{m}(1-\varepsilon)}{N}\,\mathrm{d}C_{\mathrm{s},i} + \frac{V_\mathrm{m}\varepsilon}{N}\,\mathrm{d}C_i \tag{1b}$$

$$C_{N-1}\,\mathrm{d}V - C_N\,\mathrm{d}V = \frac{V_\mathrm{m}(1-\varepsilon)}{N}\,\mathrm{d}C_{\mathrm{s},N} + \frac{V_\mathrm{m}\varepsilon}{N}\,\mathrm{d}C_N \tag{1c}$$

where $V$ is the effluent volume, $V_\mathrm{m}$ is the volume of the column or membranes, $N$ is the number of theoretical plates, $\varepsilon$ is the porosity, $C$ and $C_\mathrm{s}$ are the solute concentration in the mobile and stationary phases, respectively. The number in the subscript denotes the index of theoretical plates.

By summing up above equations, we obtain:

$$C_0 - C_N = \frac{V_\mathrm{m}(1-\varepsilon)}{N}\sum_{i=1}^{N}\frac{\mathrm{d}C_{\mathrm{s},i}}{\mathrm{d}V} + \frac{V_\mathrm{m}\varepsilon}{N}\sum_{i=1}^{N}\frac{\mathrm{d}C_i}{\mathrm{d}V} \tag{2}$$

Because the inlet concentration is kept constant, the change rate of solute concentration in the mobile and stationary phases in each plate, $\mathrm{d}C_i/\mathrm{d}V$ and $\mathrm{d}C_{\mathrm{s},i}/\mathrm{d}V$, may be assumed to decrease to zero with increasing effluent volume. From a certain time when the adsorption in the first several plates reaches saturation, the breakthrough curve may mainly reflect the process in the last plate. In this case, Eq. (2) may be simplified as:

$$C_0 - C_N \approx \frac{V_\mathrm{m}(1-\varepsilon)}{N}\frac{\mathrm{d}C_{\mathrm{s},N}}{\mathrm{d}V} + \frac{V_\mathrm{m}\varepsilon}{N}\frac{\mathrm{d}C_N}{\mathrm{d}V} \tag{3}$$

If the equilibrium of the solute between the mobile and stationary phases may be accounted for by Langmuir isotherm,

$$C_\mathrm{s} = \frac{C_\mathrm{l}C}{K_\mathrm{d}+C} \tag{4}$$

we obtain:

$$C_{\mathrm{s},N} = \frac{C_\mathrm{l}C_N}{K_\mathrm{d}+C_N},$$

$$\frac{\mathrm{d}C_{\mathrm{s},N}}{\mathrm{d}V} = \frac{\mathrm{d}C_{\mathrm{s},N}}{\mathrm{d}C_N}\frac{\mathrm{d}C_N}{\mathrm{d}V} = \frac{C_\mathrm{l}K_\mathrm{d}}{(K_\mathrm{d}+C_N)^2}\frac{\mathrm{d}C_N}{\mathrm{d}V} \tag{5}$$

By substituting Eq. (5) into Eq. (3), we obtain:

$$C_0 - C_N = \frac{V_\mathrm{m}(1-\varepsilon)}{N}\frac{C_\mathrm{l}K_\mathrm{d}}{(K_\mathrm{d}+C_N)^2}\frac{\mathrm{d}C_N}{\mathrm{d}V} + \frac{V_\mathrm{m}\varepsilon}{N}\frac{\mathrm{d}C_N}{\mathrm{d}V} \tag{6}$$

Eq. (6) may be rewritten as:

$$\begin{aligned}\frac{\mathrm{d}V}{V_\mathrm{m}(1-\varepsilon)} &= \frac{C_\mathrm{l}K_\mathrm{d}}{N}\frac{\mathrm{d}C_N}{(C_0-C_N)(K_\mathrm{d}+C_N)^2} + \frac{\varepsilon}{N(1-\varepsilon)}\frac{\mathrm{d}C_N}{C_0-C_N}\\ &= \frac{C_\mathrm{l}K_\mathrm{d}}{N(C_0+K_\mathrm{d})}\frac{\mathrm{d}C_N}{(K_\mathrm{d}+C_N)^2} + \frac{C_\mathrm{l}K_\mathrm{d}}{N(C_0+K_\mathrm{d})^2}\frac{\mathrm{d}C_N}{K_\mathrm{d}+C_N}\\ &\quad + \frac{1}{N}\left[\frac{C_\mathrm{l}K_\mathrm{d}}{(C_0+K_\mathrm{d})^2} + \frac{\varepsilon}{1-\varepsilon}\right]\frac{\mathrm{d}C_N}{C_0-C_N}\end{aligned} \tag{7}$$

Eq. (7) is an ordinary differential equation. With initial condition $C_N = 0$ at $V = 0$, the analytical solution of it is:

$$\begin{aligned}\frac{V}{V_\mathrm{m}(1-\varepsilon)} &= \frac{C_\mathrm{l}}{N(C_0+K_\mathrm{d})}\frac{C_N}{K_\mathrm{d}+C_N} + \frac{C_\mathrm{l}K_\mathrm{d}}{N(C_0+K_\mathrm{d})^2}\ln\left(1+\frac{C_N}{K_\mathrm{d}}\right)\\ &\quad - \frac{1}{N}\left[\frac{C_\mathrm{l}K_\mathrm{d}}{(C_0+K_\mathrm{d})^2} + \frac{\varepsilon}{1-\varepsilon}\right]\ln\left(1-\frac{C_N}{C_0}\right)\end{aligned} \tag{8}$$

If $C$ replaces $C_N$ to denote the outlet concentration and the following dimensionless groups are introduced to simplify the expressions,

$$c = \frac{C}{C_0} \tag{9a}$$

$$\lambda = \frac{C_\mathrm{l}}{C_0} \tag{9b}$$

$$\psi = \frac{C_0}{K_d} \tag{9c}$$

$$v = \frac{V}{V_m(1-\varepsilon)} = \frac{uA\varepsilon f}{LA(1-\varepsilon)}t = \frac{u\varepsilon f}{L(1-\varepsilon)}t \tag{9d}$$

Eq. (8) may be rewritten as:

$$v(c) = \frac{A(c)}{N} \tag{10}$$

where

$$A(c) = \frac{\lambda}{1+(1/\psi)}\frac{c}{(1/\psi)+c} + \frac{\lambda/\psi}{(1+(1/\psi))^2}\ln(1+\psi c) - \left[\frac{\lambda/\psi}{(1+(1/\psi))^2} + \frac{\varepsilon}{1-\varepsilon}\right]\ln(1-c)$$

From Eq. (3), it may be seen that Eq. (10) is limited to a certain late region of the breakthrough curve and cannot describe the initial region. So as to solve this problem, Eq. (10) is modified. A parameter, $v_0$, is introduced into Eq. (10) and $\alpha$ replaces $N$. This new model may be expressed as Eq. (11) and it can be used to describe the whole curve:

$$\begin{cases} c = 0, & v \le v_0 \\ v(c) = v_0 + \frac{A(c)}{\alpha}, & v > v_0 \end{cases} \tag{11}$$

Eq. (11) is called "multi-plate model" in this paper. In this model, $v_0$ may be considered as the theoretical dimensionless breakthrough volume at which the solute just reaches the outlet. It may be used as a retention value for the breakthrough curve. Parameter $\alpha$ may indicate the chromatographic performance. As shown further, it is related to the axial Peclet number ($Pe$) of the E-D model or the dimensionless association rate coefficient ($\mu$) of the Thomas model.

The values of $v_0$ and $\alpha$ may be obtained by fitting experimental data to Eq. (11). The sum of residuals between experimental and theoretical values is defined in Eq. (12) and then minimized:

$$Y = \sum_i \left[1 - \frac{v(c_{ex,i})}{v_{ex,i}}\right]^2 \tag{12}$$

From equations

$$\begin{cases} \dfrac{\partial Y}{\partial v_0} = -2\sum_i \dfrac{1}{v_{ex,i}}\left[1 - \dfrac{v_0 + A(c_{ex,i})/\alpha}{v_{ex,i}}\right] = 0 \\ \dfrac{\partial Y}{\partial \alpha} = \dfrac{2}{\alpha^2}\sum_i \dfrac{A(c_{ex,i})}{v_{ex,i}}\left[1 - \dfrac{v_0 + A(c_{ex,i})/\alpha}{v_{ex,i}}\right] = 0 \end{cases}$$

we obtain:

$$\begin{cases} v_0 \sum \dfrac{1}{v^2} + \dfrac{1}{\alpha}\sum \dfrac{A(c_{ex,i})}{v_{ex,i}^2} = \sum \dfrac{1}{v_{ex,i}} \\ v_0 \sum \dfrac{A(c_{ex,i})}{v_{ex,i}^2} + \dfrac{1}{\alpha}\sum \dfrac{A^2(c_{ex,i})}{v_{ex,i}^2} = \sum \dfrac{A(c_{ex,i})}{v_{ex,i}} \end{cases}$$

By solving above equations simultaneously, we obtain:

$$v_0 = \frac{\sum_i A(c_{ex,i})/v_{ex,i}\sum_i A(c_{ex,i})/v_{ex,i}^2 - \sum_i 1/v_{ex,i}\sum_i A^2(c_{ex,i})/v_{ex,i}^2}{\left[\sum_i A(c_{ex,i})/v_{ex,i}^2\right]^2 - \sum_i 1/v_{ex,i}^2\sum_i A^2(c_{ex,i})/v_{ex,i}^2} \tag{13}$$

$$\alpha = \frac{\left[\sum_i A(c_{ex,i})/v_{ex,i}^2\right]^2 - \sum_i 1/v_{ex,i}^2\sum_i A^2(c_{ex,i})/v_{ex,i}^2}{\sum_i A(c_{ex,i})/v_{ex,i}^2\sum_i 1/v_{ex,i} - \sum_i 1/v_{ex,i}^2\sum_i A(c_{ex,i})/v_{ex,i}} \tag{14}$$

In this paper, experimental data in the range of $c$ from 0.05 to 0.95 is used to calculate $v_0$ and $\alpha$ by Eqs. (13) and (14).

In order to see how well is the correlation, the coefficient of determination (COD) is calculated as:

$$\mathrm{COD} = 1 - \frac{\sum_i (c_{ex,i} - c_{th,i})^2}{\sum_i (c_{ex,i} - \bar{c}_{ex})^2} \tag{15}$$

Finally, it should be noted that the MP model is also suited for other types of isotherm models. In these cases, the general form of the MP model is also Eq. (11), where only the expression of $A(c)$ varies with the isotherms. The expression of $A(c)$ may be obtained by solving the following ordinary different equation with the isotherm and the initial condition,

$$1 - c = \frac{dq}{dv} + \frac{\varepsilon}{1-\varepsilon}\frac{dc}{dv} \tag{16}$$

For example, with the linear isotherm, $q = Kc$, and the initial condition $c = 0$ at $v = 0$, the expression of $A(c)$ may be obtained as:

$$A(c) = -\left(K + \frac{\varepsilon}{1-\varepsilon}\right)\ln(1-c) \tag{17}$$

### 2.2. Equilibrium-dispersive model

The mass balance equation of the E-D model is:

$$\frac{\partial C}{\partial t} + \frac{1-\varepsilon}{\varepsilon}\frac{\partial C_s}{\partial t} = D\frac{\partial^2 C}{\partial Z^2} - u\frac{\partial C}{\partial Z} \tag{18}$$

In the E-D model, the equilibrium of the solute between mobile and stationary phases is assumed to be fast enough and it is accounted for by Langmuir isotherm (Eq. (4)) in this paper. The initial and boundary conditions are [4,12]:

$$C = 0, \quad C_s = 0 \quad \text{at} \quad t = 0, \quad 0 \le Z \le L \tag{19}$$

$$uC_0 = uC - D\frac{\partial C}{\partial Z} \quad \text{at} \quad t > 0, \quad Z = 0 \tag{20}$$

$$\frac{\partial C}{\partial Z} = 0 \quad \text{at} \quad t > 0, \quad Z = L \tag{21}$$

By substituting Eqs. (9a)–(9d) and defining:

$$z = \frac{Z}{L} \tag{22}$$

$$q = \frac{C_s}{C_0} \tag{23}$$

Eqs. (4), (18) and (19)–(21) may be rewritten as:

$$\frac{\varepsilon f}{1-\varepsilon}\frac{\partial c}{\partial v} + f\frac{\partial q}{\partial v} = \frac{1}{Pe}\frac{\partial^2 c}{\partial z^2} - \frac{\partial c}{\partial z} \tag{24}$$

$$q = \frac{\lambda c}{(1/\psi) + c} \tag{25}$$

$$c = 0, \quad q = 0 \quad \text{at} \quad v = 0, \quad 0 \le z \le 1 \tag{26}$$

$$1 = c - \frac{1}{Pe}\frac{\partial c}{\partial z} \quad \text{at} \quad z = 0, \quad v > 0 \tag{27}$$

$$\frac{\partial c}{\partial z} = 0 \quad \text{at} \quad z = 1, \quad v > 0 \tag{28}$$

where $Pe$ is the axial Peclet number, $Pe = uL/D$. With the E-D model, we may calculate the number of theoretical plates by [20]:

$$N = \tfrac{1}{2} Pe \tag{29}$$

### 2.3. Thomas model

In the Thomas model, the effect of axial dispersion is ignored, i.e. $D$ is set to be zero in Eqs. (18) and (20), and the sorption kinetics is expressed as:

$$\frac{dC_s}{dt} = k_1 C(C_l - C_s) - k_2 C_s \tag{30}$$

The analytical solution of the Thomas model is [12,16]:

$$c(z=1) = \frac{J(n/r, nT)}{J(n/r, nT) + [1 - J(n, nT/r)]\,\exp[(1-1/r)(n-nT)]} \tag{31}$$

where

$$n = \frac{1-\varepsilon}{\varepsilon}\frac{C_l k_1 L}{u} = \frac{1-\varepsilon}{\varepsilon}\mu \tag{32}$$

$$r = 1 + \frac{C_0}{K_d} = 1 + \psi \tag{33}$$

$$T = \frac{\varepsilon K_d r}{(1-\varepsilon)C_l}\left(\frac{ut}{L} - 1\right) = \frac{1+\psi}{\lambda\psi}\left(\frac{v}{f} - \frac{\varepsilon}{1-\varepsilon}\right) \tag{34}$$

The $J$ function in Eq. (31) is defined as:

$$J(x, y) = 1 - \exp(-y)\int_0^x \exp(-\eta) I_0(2\sqrt{\eta y})\, d\eta \tag{35}$$

where $I_0$ is the modified Bessel function of zeroth order.

Parameter $\mu$ in Eq. (32) may be taken as the ratio of possible maximum concentration of the solute in the stationary phase ($C_s = C_l k_1 C_0 L/u$) and feed concentration ($C_0$) at hold-up time ($L/u$). When $\mu$ is larger, the predicted curve is closer to the ideal case. So it may also be used to indicate chromatographic performance that is similar to $Pe$.

## 3. Experimental

### 3.1. Equipment

MAC was performed on an automated Econo system (Bio-Rad, CA, USA) comprising an EP-1 pump, an EM-1 UV monitor, an ES-1 system controller and an SV-3 diverter valve. Response of the detector was recorded by Chromatography Station for Windows software (Jiangshen, Dalian, China). RPLC was performed on an HPLC system (JASCO, Japan) consisting of an LG-1580-04 low-pressure gradient unit, a DG-1580-54 degasser, a PU-1580 pump, a UV-1575 detector. Response of the detector was recorded by CKChrom chromatography data system (American Sage Inc., CA, USA). The colorimetric method was performed on a V-550 UV–vis spectrophotometer (Jasco, Japan).

### 3.2. Materials

Membrane holder (inner diameter 47 mm) was gifted by Kefen (Dalian, China). Cellulose filters were purchased from Xinhua Paper Plant (Hangzhou, Zhejiang, China). Cibacron blue F3GA was purchased from Serva (Heidelberg, Germany). Bovine serum albumin (BSA), Fraction V (purity ≥98%) was purchased from Amresco (Solon, OH, USA). Coomassie brilliant blue G250 was purchased from Fluka (Buchs, Switzerland). Kromasil $C_{18}$-silica gel was purchased from Akzo Nobel (Sweden). Caffeine (purity 98.5–100.5%) was purchased from Acros Organics (Belgium). HPLC-grade methanol was purchased from Yuchen Chemical Plant (Shandong, China).

### 3.3. Chromatographic conditions

Cellulose filters were cut into discs of 47 mm diameter. Then, cibacron blue F3GA was immobilized onto them according to the procedure published elsewhere [21]. In the operation of MAC, 15 pieces of cibacron blue F3GA-modified cellulose membranes were sealed in the membrane holder and then connected into Econo system. BSA was selected as the solute. The buffer for the loading and washing stages was 0.2 M NaCl–0.05 M NaAc buffer (pH 4.0). The elution buffer was 0.2 M KSCN–0.05 M phosphate buffer (pH 8.0). The protein absorbance was monitored at 280 nm. The operation was performed at room temperature. A solution of BSA in the elution buffer was used to determine the hold-up time. The porosity of affinity membranes was measured using a published method [22].

In the operation of RPLC, $C_{18}$-silica gel was packed into a stainless steel column (15 cm × 0.46 cm). The mobile phase

Table 1
Parameters for isotherm determination of caffeine

| Stage | Concentration (mg mL$^{-1}$) | Detection wavelength (nm) |
|---|---|---|
| 1 | 0.001–0.01 | 272 |
| 2 | 0.01–0.1 | 245 |
| 3 | 0.1–1 | 300 |
| 4 | 1–10 | 306 |

was methanol–water (25:75) and the solute was caffeine. The operation was also performed at room temperature. After each determination of the breakthrough curve, the column was washed with adequate methanol and then equilibrated with the mobile phase. Uracil was used as an inert tracer with methanol as mobile phase to determine the column void volume and extracolumn void volume [9].

### 3.4. Adsorption isotherm measurements

The adsorption isotherm of BSA onto cibacron blue F3GA affinity membranes was measured by a batch method. In experiment, 0.2 g of membranes were immersed into 10 mL of BSA loading buffer solutions having different concentrations. Then, they were shaken for 24 h at room temperature. The protein concentrations were measured by Coomassie brilliant blue method [23]. The amount of protein adsorbed onto membranes was calculated from difference between the initial concentration and that after adsorption.

The adsorption isotherm of caffeine onto $C_{18}$-bonded silica gel was measured by staircase method of FA [4]. FA experiments were performed in four separate stages as detailed in Table 1. Each stage corresponded to 10 steps and each step increased in concentration by 10% increments of the maximum concentration in the stage. The amount adsorbed on the stationary phase at step $i$ is calculated according to Eq. (36) [24]:

$$C_{s,i} = C_{s,i-1} + \frac{(C_i - C_{i-1})(V_{F,i} - V_0)}{V_a} \quad (36)$$

The adsorption amount of caffeine in first step of a higher concentration range was found to agree with that in the lower range, and was used as the basis for other successive steps due to less accumulated error in it. Then, individual stages were spliced together to construct the overall adsorption isotherm. The first step in each range was deleted from the overall isotherm plot due to overlap with the previous range [8].

### 3.5. Computational

Isotherm data were fitted to the Langmuir isotherm using nonlinear fitting procedure with Origin 6.1 software (OriginLab, MA, USA). The MP model was calculated by using Microsoft Excel. The solution of the E-D model was calculated using finite difference method [25]. A forward difference is used for the convection term in the predictor step, and a backward difference in the corrector step. Central difference is used for the diffusion term. The calculation error made is of second order. This algorithm was programmed in the laboratory in Visual Basic code. The Thomas model was calculated by using Mathematica 4.0 software (Wolfram Research, IL, USA). All the calculations were completed on a 1.5 GHz Pentium IV computer.

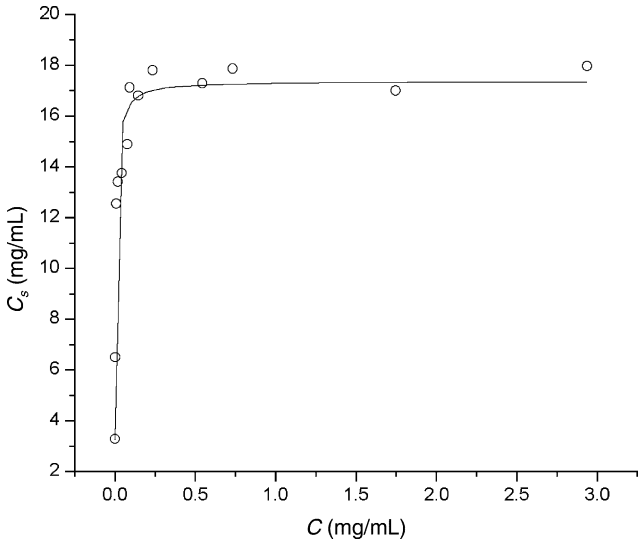


Fig. 1. Langmuir isotherm of BSA on cibacron blue F3GA cellulose membranes.

## 4. Results and discussion

### 4.1. Adsorption isotherms

Fig. 1 shows equilibrium isotherm data of BSA on cibacron blue F3GA cellulose membranes. Fig. 2 shows that of caffeine on Kromasil $C_{18}$-bonded silica column. These

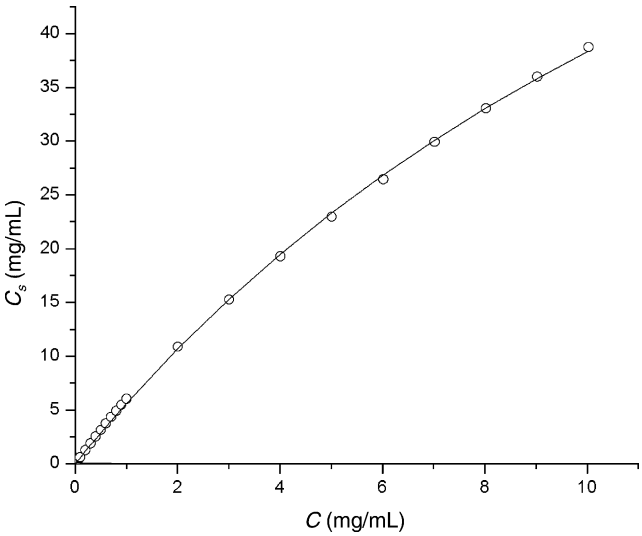


Fig. 2. Langmuir isotherm of caffeine on Kromasil $C_{18}$-bonded silica gel. Data points for lowest two concentration ranges are unobservable in this figure.

Table 2
Values of parameters used in simulating experimental breakthrough curves

| Parameter | For MAC | For RPLC |
|---|---|---|
| Capacity, $C_1$ (mg mL$^{-1}$) | 17.38 | 108.6 |
| Dissociation equilibrium constant, $K_d$ (mg mL$^{-1}$) | 0.00517 | 18.34 |
| Porosity, $\varepsilon$ | 0.77 | 0.62 |
| Length, $L$ (cm) | 0.324 | 15.0 |
| Feed concentration, $C_0$ (mg mL$^{-1}$) | 1.0 | 1.0 |
| Volumetric flow rate, $U$ (mL min$^{-1}$) | 1.0 | 1.0 |
| Correction factor, $f$ | 0.41 | 1.0 |

data are both well accounted for by the Langmuir isotherm (Eq. (4)). The best isotherm parameters obtained by nonlinear fitting procedure are presented in Table 2. Other parameters that are used in simulating the experimental breakthrough curves are also listed in this table.

### 4.2. Comparison between the MP and E-D models

In the E-D model, all contributions leading to band broadening are lumped into the apparent dispersion coefficient. In order to see how well the MP model can show the effect of the dispersion, simulated curves were first calculated by using the E-D model and then fitted to the MP model. In this investigation, $\lambda$ and $\psi$ were both varied from 0.5 to 200 to represent different systems. The value of *Pe* was from 2 to 5000. The values of $\varepsilon$ and $f$ were set at 0.6 and 1, respectively. About 2000 cases were analyzed and an example of the fittings is shown in Fig. 3.

It was found that most of simulated curves could be well fitted to the MP model. The values of COD were varied from 0.98 to 1.00. This good correlation shows that the MP model can well accommodate the type of band broadening that is comprised of diffusion-dominated processes. A typical relationship between their parameters is shown in Fig. 4.

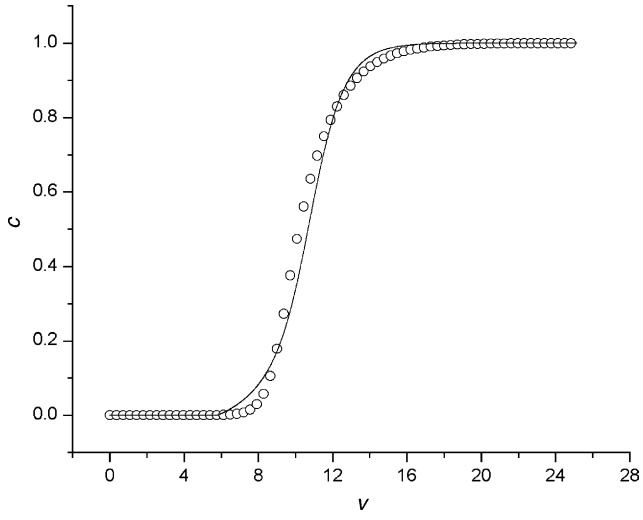


Fig. 3. Fittings of simulated data calculated by the E-D model (open circle) to the MP model (solid line). The values of $\lambda$ and $\psi$ are both 10 and *Pe* is 2. COD of the fitting is 0.993.

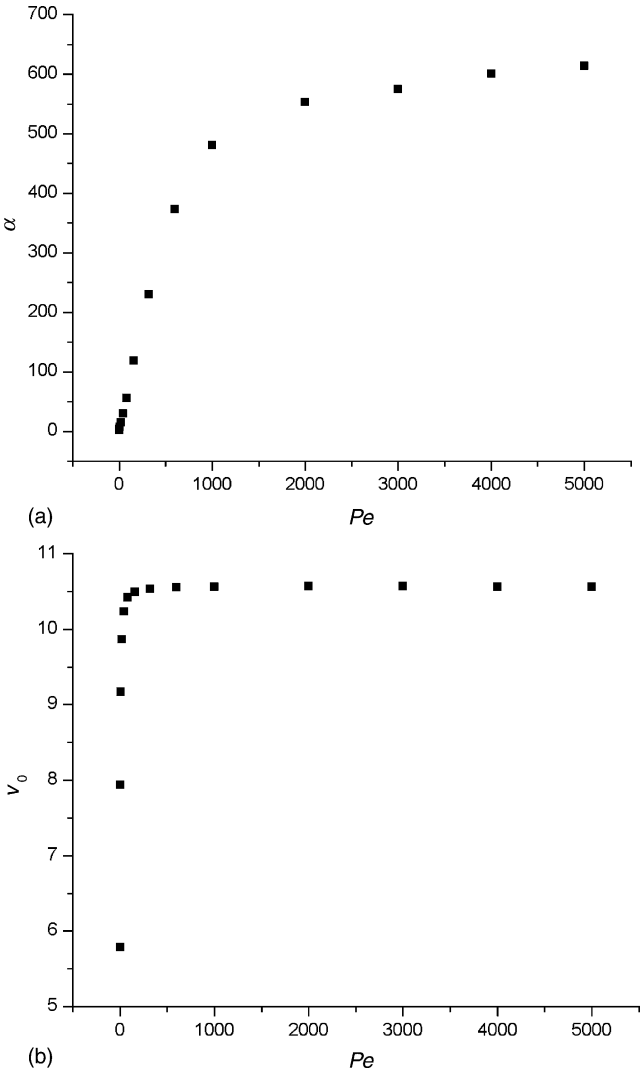


Fig. 4. Relationships between parameters of the MP and E-D models where $\lambda = 10$ and $\psi = 10$. (a) Relationship between $\alpha$ and *Pe*. (b) Relationship between $v_0$ and *Pe*.

In Fig. 4, the change rate of $\alpha$ and $v_0$ will decrease gradually with increasing *Pe*. This result shows that the difference between the simulated curves calculated by the E-D model is becoming smaller when *Pe* is larger. As shown in the literatures [12,15,26,27], the effect of axial dispersion to broaden the breakthrough curve will be insignificant when *Pe* is more than about 40. This is also confirmed by the result in our study that the curve plotted by $\alpha$ versus *Pe* or $v_0$ versus *Pe* will become convex when *Pe* is more than 40. In the range where *Pe* is below 40, there is a good linear relationship between *Pe* and $\alpha$. Some results showing this relationship are presented in Table 3. No similar linear relationship was found between $v_0$ and *Pe*. The value of $v_0$ turns out to increase faster than $\alpha$ with increasing *Pe* and reaches a constant eventually. If $v_0$ is taken as the retention value, the "saturation" of it shows that this value will be determined mainly by thermodynamics when *Pe* is large enough. This may be used to explain the

Table 3
Linear relationships between *Pe* and $\alpha$ in the range of *Pe* from 2 to 40

| $\lambda$ | $\psi$ | Regression equation | Correlation coefficient |
|---|---|---|---|
| 100 | 1 | $\alpha = 0.8051 + 0.2987Pe$ | 0.9996 |
| 10 | 10 | $\alpha = 0.4253 + 0.7456Pe$ | 0.9999 |
| 1 | 100 | $\alpha = 0.3755 + 0.3486Pe$ | 0.9978 |

reason of the success for the equilibrium model to predict the band profiles [7,9].

### 4.3. Comparison between the MP and Thomas models

In the Thomas model, all contributions leading to band broadening are lumped into the association rate coefficient. In order to see how well the MP model can show the effect of sorption kinetics, simulated curves calculated by using the Thomas model were fitted to the MP model. In this investigation, $\lambda$ and $\psi$ were varied from 0.5 to 200 and $\mu$ was from 1 to 3200. The values of $\varepsilon$ and $f$ were set at 0.6 and 1, respectively. In addition, because the outlet concentration before the hold-up time is equal to zero in the Thomas model, an abrupt increase of it at this time will be found when the sorption kinetics is much slower. Therefore, only simulated data after the hold-up time were fitted to the MP model and used to calculate COD. About 2000 cases were analyzed and an example of the fittings is shown in Fig. 5.

Most of simulated curves calculated by the Thomas model could be well fitted to the MP model and COD were varied from 0.98 to 1.00. This result also shows that the MP model can well accommodate the type of band broadening that is comprised of kinetic sorption processes. A typical relationship between these parameters is shown in Fig. 6. In this figure, similar to the relationship between $v_0$ and *Pe*, $v_0$ reaches a constant quickly with increasing $\mu$. However, it is different

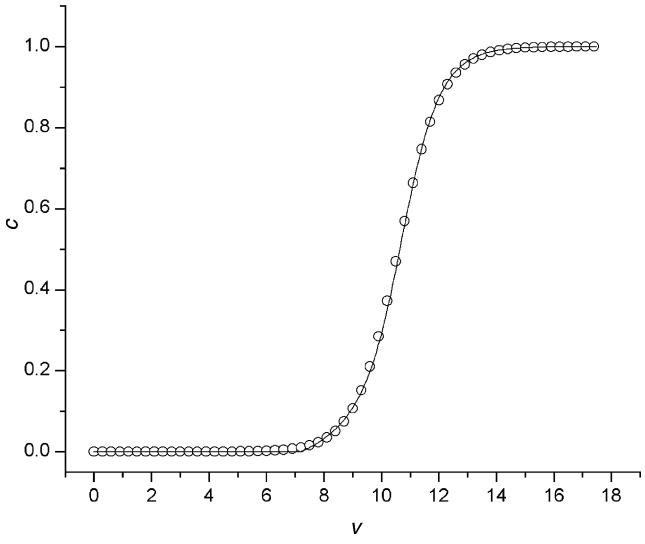


Fig. 5. Fittings of simulated data calculated by the Thomas model (open circle) to the MP model (solid line). The values of $\lambda$ and $\psi$ are both 10 and $\mu$ is 20. COD of the fitting is 0.999.

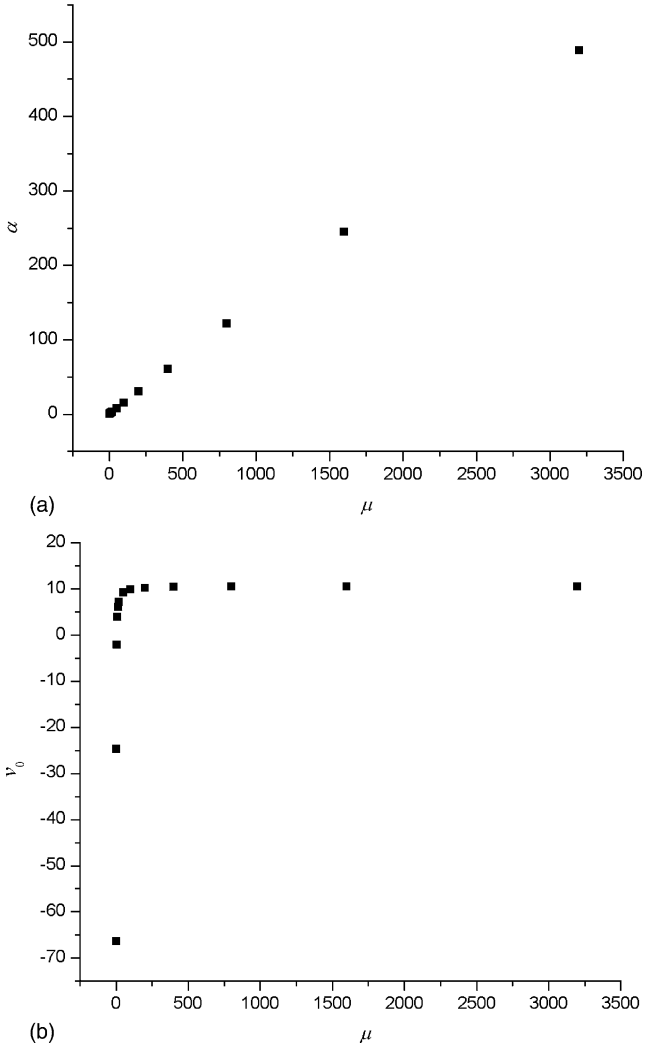


Fig. 6. Relationships between parameters of the MP and Thomas models where $\lambda = 10$ and $\psi = 10$. (a) Relationship between $\alpha$ and $\mu$. (b) Relationship between $v_0$ and $\mu$.

Table 4
Linear relationships between $\mu$ and $\alpha$ in the range of $\mu$ from 1 to 3200

| $\lambda$ | $\psi$ | Equation | Correlation coefficient |
|---|---|---|---|
| 100 | 1 | $\alpha = 0.0021 + 0.1411\mu$ | 0.9999 |
| 10 | 10 | $\alpha = -0.0193 + 0.6139\mu$ | 0.9999 |
| 1 | 100 | $\alpha = 0.7161 + 0.0.5565\mu$ | 0.9999 |

from the relationship between $\alpha$ and *Pe* that $\alpha$ depends linearly on $\mu$ in a much wider range. Some results showing this linear relationship are presented in Table 4.

### 4.4. Application of the MP model in MAC

As validation of its practical use, the MP model was applied to describe experimental breakthrough curves that were obtained from the adsorption of BSA on cibacron blue F3GA cellulose membranes. As comparison, the fittings of experimental data to the E-D and Thomas models were also ob-

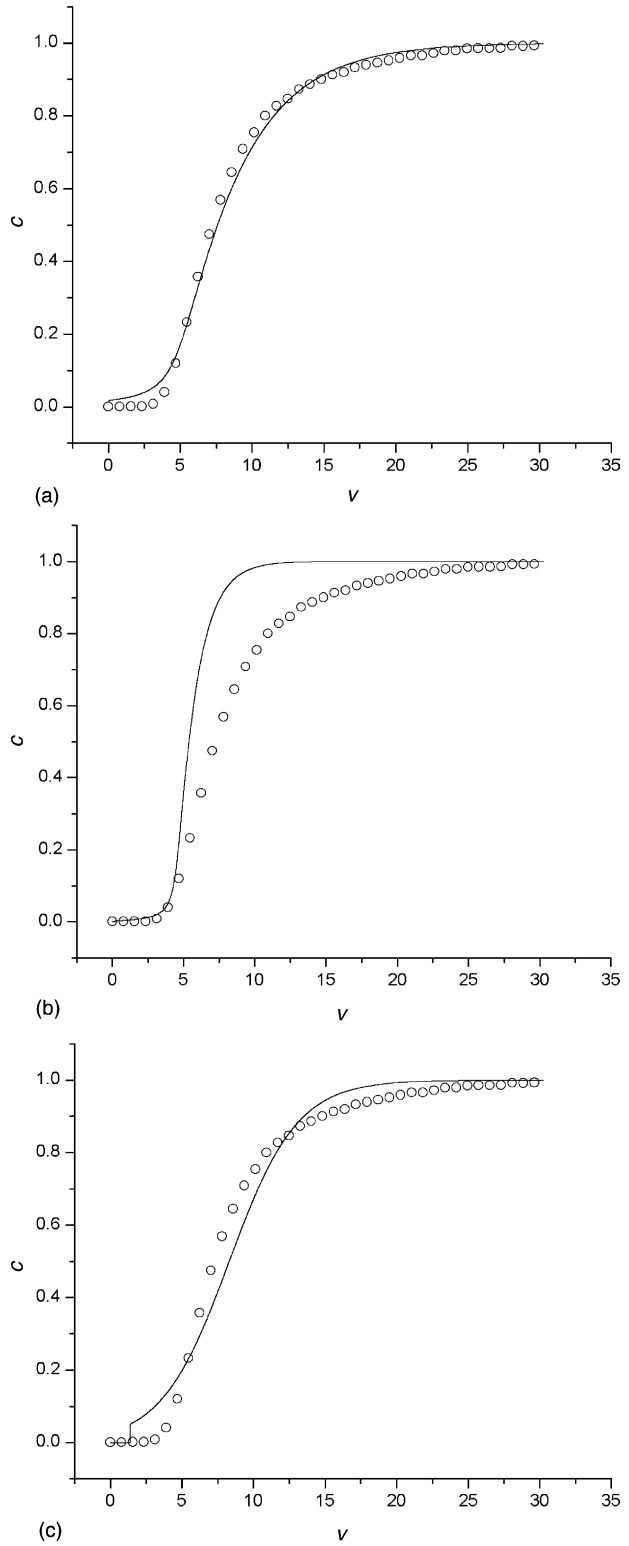


Fig. 7. Fittings of experimental breakthrough curve (open circle) obtained in MAC to: (a) MP model; (b) E-D model; (c) Thomas model.

tained by changing the values of *Pe* and $\mu$ to make the error be the least between experimental and theoretical values. The fittings are shown in Fig. 7 and corresponding values of COD are presented in Table 5.

Table 5
Values of COD for the fittings of experimental breakthrough curves to the models

| | MAC | RPLC |
|---|---|---|
| MP model | 0.996 | 0.999 |
| E-D model | 0.821 | 0.998 |
| Thomas model | 0.978 | 0.997 |

The experimental breakthrough curve is well fitted to the MP model. However, the discrepancy between it and the theoretical curve calculated by the E-D model turns out to be significant. This result is as expected, because the E-D model will not be suited for affinity separations where the kinetics are slow [28–31]. The Thomas model concerns the effect of sorption kinetics and has been used to describe the breakthrough curves obtained in MAC [12,18]. In our study, the fitting of the experimental curve to the Thomas model is indeed better than that to the E-D model. However, there is also a little discrepancy between experimental and theoretical values calculated by this model, which is similar to the result of Sarfert and Etzel [18]. This discrepancy perhaps is due to the existence of heterogeneous flow distribution in the system. In the Thomas model, it is assumed that the flow regime be the plug flow mode. However, this may not be true in MAC, which is mainly due to the low packing density for membrane modules [32–34]. Retarded flow will influence the shape of the breakthrough curve significantly and the one-dimensional Thomas model seems not to be capable of explaining this effect. It seems necessary to use two- or three-dimensional chromatographic models to explain the experimental results. However, the use of these models will somewhat complicated the analysis and it will not be handy to chromatographers. From this case, it is shown that the MP model may lump this effect in a simplified manner into its model parameters.

### 4.5. Application of the MP model in RPLC

The E-D, Thomas and MP models were also applied to describe the breakthrough curves that were obtained from the adsorption of caffeine on $C_{18}$-bonded silica column. The fittings are shown in Fig. 8 and the values of COD are presented in Table 5. In this case, all the models may well describe the experimental curve.

As shown earlier $\alpha$ is related to *Pe* and $\mu$. Therefore, according to this relationship, another approach may be proposed to estimate the coefficients of mass transfer from experimental data. For example, in order to find the best $\mu$, some values of $\alpha$ may be obtained beforehand by fitting the simulated curves, which are calculated by using the Thomas model with different values of $\mu$ as well as other experimental parameters, to the MP model. These $\alpha$ and $\mu$ may be used to construct a "standard curve" and a regression equation may be obtained to describe the relationship between them. In the analysis of experimental data, $\alpha$ may be first calculated by using Eqs. (13) and (14) and then $\mu$ read from the standard

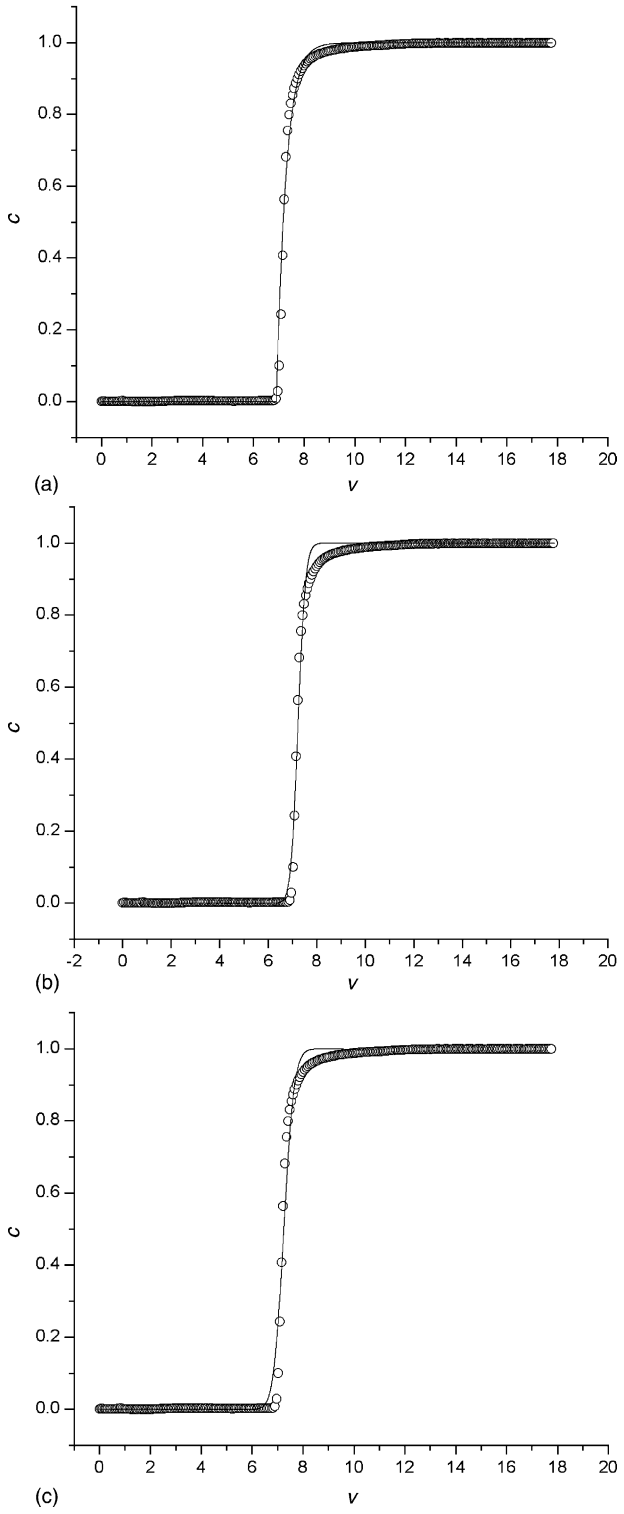


Fig. 8. Fittings of experimental breakthrough curve (open circle) obtained in RPLC to: (a) MP model; (b) E-D model; (c) Thomas model.

curve or calculated by the equation. Analogously, the best *Pe* for experimental data may also be found. With this approach, we obtained the fittings of the experimental curve to the E-D and the Thomas models that are presented in Fig. 8(b) and (c). These results show the reliability of this approach.

The approach mentioned above may give chromatographers a convenient way to investigate the influence of factors such as column loading and flow rate on the nonlinear chromatographic performance. Once the adsorption isotherm is determined, the standard curve showing the relationship between $\alpha$ and *Pe* or $\mu$ may be plotted beforehand. In practice, $\alpha$ may be first readily calculated by making graphic measurement and applying simple equations, and then corresponding *Pe* or $\mu$ directly read from the curve. This approach may avoid the work that had to be done by changing *Pe* or $\mu$ at each concentration or flow rate to find the best agreement between experimental and theoretical values. It will reduce the calculation and save time as possible especially when the amount of experimental data is large. Also the accuracy of this approach is reliable. If more precise values of *Pe* and $\mu$ is required, the values calculated by this approach may be taken as the initial guess for nonlinear fitting procedures that are programmed with simplex or Levenberg–Marquardt algorithms [4,35]. No other initial guesses are needed to avoid the possible false optimal values. Moreover, in some cases where one only wants to know the relationship between the performance and feed concentration or flow rate, the MP model may be a good choice because $\alpha$ may be used to indicate the performance and this model will be easier and faster to process experimental data. In a word, the MP model may be a complementary approach for the study of nonlinear chromatography. It will be useful especially when the E-D and Thomas models cannot give satisfactory description to experimental data.

## 5. Conclusions

A new mathematical model, MP model, is proposed by FA to evaluate nonlinear chromatographic performance. A good correlation was found between it and the E-D or Thomas models. Therefore, this model may be used to obtain information about band broadening effects such as dispersion and sorption effects. The MP model may well describe experimental breakthrough curves that are obtained in MAC and RPLC. It is simple and fast to process experimental data. Moreover, the relationship between it and the E-D or Thomas models may be used to calculate the coefficients of mass transfer. This approach may reduce the calculation as possible and be applied to study the effects such as column loading and flow rate. The limitation of the MP model is that it is confined to FA and cannot be used to describe the elution band profiles.

## Nomenclature

| | |
|---|---|
| $A$ | section area ($cm^2$) |
| $c$ | dimensionless solute concentration in the mobile phase |
| $\bar{c}$ | average of dimensionless outlet concentration |

| | |
|---|---|
| $C$ | solute concentration in the mobile phase (mg mL$^{-1}$) |
| $C_0$ | feed concentration (mg mL$^{-1}$) |
| $C_l$ | maximum capacity of adsorbent (mg mL$^{-1}$) |
| $C_s$ | solute concentration in the solid phase (mg mL$^{-1}$) |
| COD | coefficient of determination |
| $D$ | apparent axial dispersion coefficient (cm$^2$ s$^{-1}$) |
| $f$ | correction factor ($f = U/uA\varepsilon$) |
| $k_1$ | association rate coefficient ((mg mL$^{-1}$)$^{-1}$ min$^{-1}$) |
| $k_2$ | dissociation rate coefficient (min$^{-1}$) |
| $K$ | partition coefficient |
| $K_d$ | dissociation equilibrium constant (mg mL$^{-1}$) |
| $L$ | Length of column or membranes (cm) |
| $N$ | number of theoretical plates |
| $Pe$ | axial Peclet number |
| $q$ | dimensionless solute concentration in the solid phase |
| $u$ | interstitial flow rate (cm min$^{-1}$) |
| $v$ | dimensionless effluent volume |
| $v_0$ | parameter of MP model |
| $V$ | effluent volume (mL) |
| $V_0$ | total void volume (mL) |
| $V_a$ | volume of adsorbent (mL) |
| $V_F$ | breakthrough volume (mL) |
| $V_m$ | volume of the column or membranes (mL) |
| $z$ | dimensionless axial distance |
| $Z$ | axial distance along membranes or column (cm) |

*Greek letters*

| | |
|---|---|
| $\alpha$ | parameter of MP model |
| $\varepsilon$ | porosity |
| $\lambda$ | dimensionless maximum capacity of adsorbent |
| $\mu$ | dimensionless association rate coefficient |
| $\psi$ | dimensionless association equilibrium constant |

*Subscripts*

| | |
|---|---|
| $i$ | index |
| ex | experimental value |
| th | theoretical value |

## References


[1] H. Chase, J. Chromatogr. 297 (1984) 179.
[2] F. Arnold, H. Blanch, C. Wilke, Chem. Eng. J. 30 (1985) 9.
[3] K. Gebauer, J. Thommes, M. Kula, Chem. Eng. Sci. 52 (1997) 405.
[4] P. Sajonz, G. Zhong, G. Guiochon, J. Chromatogr. A 731 (1996) 1.
[5] G. Shay, G. Szelkey, Acta Chim. Hung. 5 (1954) 167.
[6] D. James, C. Phillips, J. Chem. Soc. (1954) 1066.
[7] O. Lisec, P. Hugo, A. Seidel-Morgensern, J. Chromatogr. A 908 (2001) 19.
[8] B. Stanley, J. Krance, A. Roy, J. Chromatogr. A 865 (1999) 97.
[9] B. Stanley, T. Savage, J. Geraghty, Anal. Chem. 70 (1998) 1610.
[10] R. Gutsche, H. Yoshida, Chem. Eng. Sci. 49 (1994) 179.
[11] P. Jandera, S. Buncekova, K. Mihlbachler, G. Guiochon, V. Backovska, J. Planeta, J. Chromatogr. A 925 (2001) 19.
[12] S. Suen, M. Etzel, Chem. Eng. Sci. 47 (1992) 1355.
[13] S. Suen, M. Caracotsios, M.R. Etzel, Chem. Eng. Sci. 48 (1993) 1801.
[14] S. Suen, M. Etzel, J. Chromatogr. A 686 (1994) 179.
[15] K. Miyabe, G. Guiochon, J. Chromatogr. A. 890 (2000) 211.
[16] H. Thomas, J. Am. Chem. Soc. 66 (1944) 1664.
[17] G. Serafica, J. Pimbley, G. Belfort, Biotechnol. Bioeng. 43 (1994) 21.
[18] F. Sarfert, M. Etzel, J. Chromatogr. A 764 (1997) 3.
[19] J. Van Deemter, F. Zuiderweg, A. Klinkenberg, Chem. Eng. Sci. 5 (1956) 271.
[20] D. Zhou, K. Kaczmarski, A. Cavazzini, X. Liu, G. Guiochon, J. Chromatogr. A 1020 (2003) 199.
[21] J. Li, J. Wang, X. Liu, Chromatographia 56 (2002) 401.
[22] W. Guo, E. Ruckenstein, J. Membr. Sci. 182 (2001) 227.
[23] M. Bradford, Anal. Biochem. 72 (1976) 248.
[24] B. Stanley, J. Krance, J. Chromatogr. A 1011 (2003) 11.
[25] P. Sajonz, G. Zhong, G. Guiochon, J. Chromatogr. A 728 (1996) 15.
[26] D. Josic, A. Buchacher, A. Jungbauer, J. Chromatogr. B 752 (2001) 191.
[27] G. Heeter, A. Liapis, J. Chromatogr. A 711 (1995) 3.
[28] A. Hunter, G. Carta, J. Chromatogr. A 897 (2000) 81.
[29] A. Hunter, G. Carta, J. Chromatogr. A 930 (2001) 79.
[30] A. Cavazzini, G. Bardin, K. Kaczmarski, P. Szabelski, M. Al-Bokari, G. Guiochon, J. Chromatogr. A 957 (2002) 111.
[31] H. Guan-Sajonz, P. Sajonz, G. Zhong, G. Guiochon, Biotechnol. Prog. 12 (1996) 380.
[32] O. Reif, R. Freitag, J. Chromatogr. A 654 (1993) 29.
[33] E. Klein, J. Membr. Sci. 179 (2000) 1.
[34] D. Roper, E. Lightfoot, J. Chromatogr. A 702 (1995) 3.
[35] J. Wade, A. Bergold, P. Carr, Anal. Chem. 59 (1987) 1286.